Study of possible local quasars II. A sample of 225 QSOs

K. P. Panov, D. P. Dimitrov

Institute of Astronomy, Bulgarian Academy of Sciences 72, Tsarigradsko Shosse blvd, 1784 Sofia, Bulgaria

Abstract. We present a study of 225 quasars in the vicinity of 18 low redshift active galaxies. Our aim is to check the conclusions of Paper I on the basis of larger sample of local quasars. The study is based on several assumptions: quasars of this sample are ejected from respective parent galaxy, i.e. they are local quasars; quasars are compact bodies with dimensions close to their respective gravitational radius; the major part of each quasar-red shift is due to gravitational reddening, i.e. they are intrinsic in origin, and gravitational redshifts are quantized according to the Karlsson-sequence. Physical characteristics of the sample quasars are obtained and several relations for local quasars are confirmed: density-redshift, absolute mag – radius, absolute mag – mass, mass – radius, mass – luminosity, and mass – density. These relations provide convincing evidence that the procedure is correct. The density – red shift relation possibly reflects evolution of quasars: with decreasing density the redshifts drop. The mass – density relation could be explained in terms of faster evolution for more massive quasars. In the process of evolution quasar density and redshift decrease, while quasar radius and luminosity increase. All relations for quasars found in Paper I are confirmed. The Arp's scenario for evolution of quasars seems to be confirmed. The end result of evolution of quasars are small mass (companion) galaxies. Decreasing density of quasars as they evolve could probably be due to disintegration of dense matter of yet unknown origin. Strong indication is found for a possible link between quasars and stars.

Keywords: Active galaxies, quasars, gravitational red shifts, evolution of quasars.

1. Introduction

The study of quasars (QSOs) began about 50 yeas ago but the most fascinating prospects seem to be yet before us. The unusually large redshifts of QSOs are unprecedented in astrophysics and different hypothesis have been proposed to explain them. The most popular theory (Standard Quasar Model – SQM) puts quasars at cosmological distances, assuming that their redshifts are due entirely to the expansion of the Universe. According to the SQM quasars are huge black holes accreting matter [1, 2, 3]. However, there is a strange consequence of this model: the larger the redshift, the larger the luminosity of the quasar. Apparent brightness of quasars seems to be decreasing more slowly with distance, indicated by their redshifts, which inevitably leads to an ever increasing luminosity (with distance). This is a problem for the SQM [4, 5]. Unresolved remains also the problem, why are there no high luminosity quasars at low redshifts? There are other problems, associated with the SQM: the number of QSOs with $z > 3$ is decreasing, while the opposite is predicted; “time – dilation” effect is not yet established beyond doubt, as it should be at cosmological distances [6, 7]. A major problem is also the Karlsson sequence – a sequence of specific and preferred values for the QSOs redshifts: 0.06, 0.30, 0.60, 0.96, 1.41, 1.96 and so on [8, 9, 10, 11]. This sequence could be obtained by the formula: $\Delta \log(1 + z) = 0.089$. Quantized redshifts mean in the framework of SQM quantized distances to quasars, and this is inconceivable. A much discussed problem during the last 40 years is the apparent association of a number of QSOs with low redshift galaxies. References on clustering of QSOs about lower redshift galaxies are quite numerous [12, 13, 14, 15, 16, 17, 18, 19, 20, 21, 22, 23]. Quasars around some active galaxies are clearly in excess and the probabilities of such associations by chance projections are very low [24]. In some cases, even physical connections between QSOs and low redshift galaxies have been detected [13]. Association of high redshift QSOs with low redshift galaxies leads inevitably to the conclusion that quasars have been ejected from the parent galaxy (or, rather, from its active nucleus, see [25, 26, 27, 28, 29]). All these difficulties prompted the idea that redshifts of quasars (or at least, the major part of the redshift) are not cosmological but intrinsic in origin. Most prominent hypothesis for the intrinsic redshifts are the gravitational reddening [30, 31, 32], and the “variable mass” hypotheses [33, 34]. The gravitational reddening follows from the theory of General Relativity. It has been considered very early in the quasar-history [30] but then abandoned for various reasons. Recently, a new attempt to revive the gravitational reddening hypothesis was done by Panov [35] = Paper I. In this study a sample of 74 local quasars was presented for which physical characteristics were calculated, and several relations were established: density – redshift, absolute mag – radius, absolute mag – mass, mass – radius, mass – luminosity, and mass – density. The density – redshift relation could probably be explained in terms of an evolution of quasars with decreasing densities and redshifts. The mass - density relation is believed to show that more massive quasars evolve fasted and the process of evolution is determined by disintegration of matter. Generally, Paper I presents evidence in favor of Arp’s evolutionary scenario for quasars [28, 36, 37, and references therein]. According to Arp’s scenario, the end product of quasar-evolution should be galaxies.

Here we present a study of 225 possible local quasars from 18 active galaxies. Our aim is to verify the conclusions of Paper I on a basis of larger sample of quasars and the Arp’s evolutionary scenario.

2. The sample of local quasars

In Table 1 the sample of local quasars is presented (data from the catalogue of Veron-Cetty and Veron ,13th ed.[38]) , where columns are self-explanatory. In the last column, the references are given to the individual studies, which were used to construct this sample.

Table 1. Sample of 225 local quasars (data from Veron-Cetty and Veron , 2010, 13 th ed.).

Galaxy redshift	Quasar	Redshift Zo	Visual mag	B-V	*References*
NGC450					
0.006	Q1= Q0107+0022	1.968	18.89	0.21	[39]
	Q2= Q0107-0235	0.958	17.80	-	
	Q3 Q0107-0232	0.728	18.85	-	
	Q4 PB6291	0.956	17.60	-	
	Q5 Q0107-025c	1.893	19.45	-	
	Q6 NGC450 No24	0.070	18.90	-	
	Q7 Q0107-001	0.468	19.38	0.09	
	Q8 Q0108-007	1.424	19.23	0.50	
	Q9 Q0108+0028	2.005	18.25	-	
	Q10 Q0108-025	1.240	18.10	-	
	Q11 Q0108-020	1.302	19.60	-	
	Q12 Q0108+001	1.003	18.67	0.26	
	Q13 Q0109-0128	1.758	18.37	0.26	
	Q14 Q0110-0107	1.896	19.29	0.22	
	Q15 Q0110-0157	1.102	17.30	-	
	Q16 PB6317	0.238	17.85	0.28	
	Q17 Q0110+004	0.910	20.08	0.21	
	Q18 Q0110-0015	0.976	18.55	-	
	Q19 Q0110-030	1.235	17.70	-	
	Q20 Q0110-0047	0.412	19.06	0.29	
	Q21 Q0110-006	0.935	19.70	-	
	Q22 Q0111-007	0.995	18.63	0.28	
	Q23 Q0111-008	0.181	18.93	0.58	
	Q24 Q0111-010	0.350	19.02	0.33	
	Q25 Q0111-005	1.908	19.45	-	
	Q26 PKS0112-017	1.365	17.50	-	
	Q27 Q0112-012	1.585	19.89	0.20	
	Q28 Q0113+000	1.279	19.19	0.37	
	Q29 Q0113-010	1.968	19.58	0.20	
	Q30 Q0113-013	2.055	19.60	-	
	Q31 Q0113-009	1.263	18.96	0.36	
	Q32 Q0114-001	1.316	18.94	0.35	
	Q33 UM314	2.190	18.32	0.22	
	Q34 UM315	2.050	18.70	-	

Galaxy redshift	Quasar	Redshift Zo	Visual mag	B-V	*References*
	Q35 Q0116-010	1.052	18.60	0.32	
	Q36 NGC450 No86	0.090	17.35	0.44	
	Q37 Q0117-023	2.019	19.80	-	
	Q38 Q0117+001	0.649	19.30	0.17	
	Q39 UM316	0.960	17.90	-	
	Q40 Q0117-012	0.202	19.13	0.65	
	Q41 NGC450 No87	0.078	19.45	-	
	Q42 Q0118-031A	1.445	18.35	-	
	Q43 Q0118-018	1.911	19.45	-	
	Q44 PB8737	1.165	18.45	-	
	Q45 PB8736	2.112	19.00	-	
	Q46 Q0118+003	0.328	19.11	0.28	
	Q47 NGC450 No217	0.135	18.75	-	
	Q48 Q0119-009	1.943	19.30	0.20	
	Q49 Q0120-001	0.909	19.21	0.37	
	Q50 Q0120-029A	1.073	18.55	-	
	Q51 Q0120-002	1.355	19.01	0.45	
	Q52 Q0120-029B	0.438	18.10	-	
	Q53 Q0120+002	0.772	19.25	-	
	Q54 Q0121+007	1.310	19.60	-	
	Q55 Q0121+009	1.555	19.04	0.33	
	Q56 Q0121-008	2.252	19.30	-	
	Q57 Q0121+008	2.043	19.50	-	
	Q58 Q0121-022	0.988	19.05	-	
	Q59 Q0122-028	2.022	19.50	-	
	Q60 Q0123-005A	1.889	19.00	-	
	Q61 Q0123-005B	1.763	18.90	0.26	
	Q62 UM322	1.930	18.40	-	
	Q63 UM324	0.355	17.35	-	
NGC613					
0.005	Q1 = 2QZJ013356-2922	2.222	20.09	-	[40]
	Q2 2QZJ013445-2928	2.059	20.32	-	
	Q3 2QZJ013454-2925	2.062	20.01	-	
	Q4 2QZJ013348-2920	1.855	20.30	-	
	Q5 2QZJ013345-2917	1.413	20.50	-	
	Q6 2QZJ013508-2930	1.482	20.31		
NGC622					[41]
0.017	Q1 = NGC622 UB1	0.910	18.36	0.32	
	Q2 = NGC622 BS01	1.460	19.13	0.20	

Galaxy redshift	Quasar	Redshift Zo	Visual mag	B-V	*References*
NGC1068					
0.003	Q1 = RXSJ02393-0001	0.261	15.48	0.30	[42]
	Q2 Q0238-0001	0.468	19.07	0.24	
	Q3 Q0238-0058	0.726	18.52	0.19	
	Q4 Q0239-0008	0.649	18.72	0.12	
	Q5 Q0239+0021	1.054	18.92	0.30	
	Q6 Q0239-0005	1.552	18.47	0.25	
	Q7 Q0239-0012	1.112	18.70	0.00	
	Q8 1WGAJ0242.1+0000	0.385	19.67	0.31	
	Q9 Q0240-0012	2.018	18.45	0.28	
	Q10 Q0241+0005	0.684	18.92	0.17	
	Q11 1WGAJ0245.5 0007	0.655	18.91	0.09	
	Q12 1WGA 0242.6+0022	0.630	20.33	0.03	
	Q13 US3137	1.139	18.44	0.34	
	Q14 US3139	1.292	18.75	0.41	
	Q15 US3146	1.815	18.63	0.19	
	Q16 Q0244-0015	2.315	20.16	0.20	
NGC1073					
0.004	Q1 = NGC1073U2	0.601	19.00	-	[43],[44]
	Q2 PKS0241+011	1.400	20.30	-	
	Q3 NGC1073U1	1.941	19.60	-	
	Q4 US3115	0.546	19.18	0.13	
NGC1097					
0.004	Q2 = Q0238-315	2.143	19.60	-	[45]
	Q3 Q0238-301	2.265	18.30	-	
	Q6 Q0238-310	2.034	19.50	-	
	Q7 Q0240-309	0.374	18.50	-	
	Q9 Q0241-316	1.588	19.90	-	
	Q10 Q0241-302	0.359	19.50	-	
	Q12 Q0242.0-3104	0.874	19.10	-	
	Q13 Q0242.1-3104	1.985	19.60	-	
	Q14 Q0242-305	1.045	18.80	-	
	Q15 Q0242.9-3010	2.269	19.90	-	
	Q16 Q0242.9-3009	0.783	19.60	-	
	Q18 Q0243.5-2946	1.577	20.20	-	
	Q19 Q0243.6-2947	2.063	20.10	-	
	Q20 Q0243-308	0.088	20.00	-	
	Q21 Q0243-318	1.875	18.50	-	
	Q23 QN1097.3	1.000	17.50	-	
	Q24 QN1097.4	0.340	18.20	-	
	Q25 QN1097.6	1.100	20.50	-	
	Q26 QN1097.5	0.887	20.00	-	

Galaxy redshift	Quasar	Redshift Zo	Visual mag	B-V	*References*
NGC2639					
0.011	Q1 = NGC2639U1	1.177	18.06	0.29	[29],[26]
	Q2 NGC2639U2	1.105	19.16	0.36	
	Q3 NGC2639U3	1.522	19.43	0.33	
	Q4 NGC2639U4	0.780	18.87	0.49	
	Q5 NGC2639U5	1.494	17.92	0.55	
	Q7 NGC2639U7	2.000	19.37	0.37	
	Q8 NGC2639U8	2.800	19.00	0.32	
	Q10 NGC2639U10	0.305	17.80	0.22	
	Q14 NGC2639U14	2.124	18.74	0.31	
	Q15 NGC2639U15	1.525	18.78	0.22	
	Q16 NGC2639 No3	0.323	18.40	0.17	
NGC3034	= M82				
0.001	Q1 = M82 No95	1.010	19.44	0.36	[46]
	Q2 = Hoag 1	2.048	19.50	0.30	
	Q3 Hoag 2	2.054	20.33	0.22	
	Q4 NGC3031U4	0.85	20.12	0.70	
	Q5 Hoag 3	2.040	20.31	0.16	
	Q6 Bol 105	2.240	21.40	-	
	Q7 M82 No69	0.930	19.38	0.70	
	Q8 M82 No22	0.960	19.04	1.31	
	Q9 Bol 75	0.740	22.00	-	
	Q10 Dahlem 7	0.675	19.80	-	
	Q11 Dahlem 12	0.626	18.90	-	
	Q12 Dahlem 17	1.086	17.99	0.33	
NGC3079					
0.004	Q1 = SBS0953+556	1.410	18.45	0.17	[47]
	Q2 4C55.17	0.898	17.89	0.35	
	Q3 SBS0955+560	1.021	17.68	0.47	
	Q4 RXJ10005+5536	0.215	19.37	0.62	
	Q5 1WGAJ1000.9+5541	1.037	19.99	0.57	
	Q6 NGC3073UB1	1.530	19.04	0.32	
	Q7 ASV1	0.072	17.28	-	
	Q8 SBS0957+557	2.102	17.60	-	
	Q9 Q0957+561A	1.413	16.95	0.21	
	Q10 Q0957+561B	1.415	16.95	0.21	
	Q11 ASV24	1.154	23.03	-	
	Q12 ASV31	0.352	21.14	-	
	Q13 MARK132	1.760	16.05	0.28	
	Q14 NGC3073UB4	1.154	18.38	0.38	
	Q15 1WGAJ1002.7+5558	0.219	21.20	-	
	Q16 Q0958+5625	3.216	20.08	-	

Galaxy redshift	Quasar	Redshift Zo	Visual mag	B-V	*References*
NGC3628					
0.003	Q1 = Wee 47	1.413	19.06	0.26	[48]
	Q2 Wee 48	2.060	18.91	0.26	
	Q3 Wee 50	1.750	19.58	0.18	
	Q4 Wee 51	2.150	19.44	0.29	
	Q8 Wee 52	2.430	20.97	0.24	
	Q9 Wee 55	1.940	19.06	0.26	
	Q10 Wee 36	2.490	20.70	-	
	Q11 Wee 38	2.370	20.05	0.48	
	Q12 Wee 45	2.100	20.12	0.08	
	Q13 Wee 37	2.140	20.02	0.55	
	Q14 Wee 40	1.740	20.09	0.13	
	Q15 Wee 34	2.320	17.85	0.65	
	Q16 Wee 46	0.060	20.20	-	
	Q17 Wee 41	2.540	20.02	0.25	
	Q18 Wee 44	2.380	19.57	0.25	
	Q19 Wee 42	2.110	20.97	0.16	
	Q20 Wee 43	3.009	19.83	0.33	
NGC4235					
0.007	Q1 = PG1216+069	0.334	15.65	-	[29]
	Q2 1ES1212+078 (BL)	0.137	16.00	-	
NGC4258					
0.002	Q1 = QJ1218+472	0.398	19.88	0.21	[25]
	Q2 QJ1219+473	0.654	19.43	0.17	
NGC4410					
0.025	Q1 = SDSSJ12260+0853	2.237	19.57	0.27	[49]
	Q2 SDSSJ12260+0912	0.662	19.24	0.09	
	Q3 SDSSJ12255+0859	1.903	19.57	0.21	
	Q5 Q1222+0901	0.535	17.29	0.10	
	Q6 SDSSJ12273+0923	1.776	19.39	0.13	
	Q8 2E1225+0858	0.085	16.64	0.38	
	Q9 SDSSJ12281+0915	1.590	20.03	0.45	
	Q10 SDSSJ12279+0922	1.502	18.82	0.26	
	Q11 SDSSJ12261+0935	0.628	19.33	0.12	
	Q12 SDSSJ12238+0856	1.043	18.74	0.30	
	Q13 SDSSJ12235+0902	1.363	19.24	0.34	
	Q15 Q1225+0836	1.471	17.59	0.30	
	Q16 SDSSJ12178+0913	1.076	19.48	0.21	
	Q17 SDSSJ12240+0935	1.345	19.32	0.24	
	Q18 SDSSJ12230+0856	1.090	19.12	0.34	
	Q19 SDSSJ12231+0914	1.715	19.49	0.09	

Galaxy redshift	Quasar	Redshift Zo	Visual mag	B-V	*References*
	Q20 Q1220+0939	0.681	17.74	0.09	
	Q21 SDSSJ12291+0938	2.649	20.08	0.33	
	Q22 SDSSJ12227+0853	0.773	18.78	0.15	
	Q23 SDSSJ12281+0951	0.064	17.72	0.65	
	Q24 Q1222+1010	0.398	18.58	0.12	
	Q25 SDSSJ12250+0955	1.429	19.04	0.26	
NGC4579					
0.005	Q2 = Q1234+1217	0.662	18.61	0.11	[50]
NGC5548					
0.017	Q1 = QJ14172+2534	0.852	18.40	-	[51]
	Q2 EXO1415.2+2607	0.184	18.03	0.32	
	Q3 QJ14182+2500	0.727	18.90	-	
	Q4 Q1408.0+2696	2.425	19.08	0.20	
	Q5 Q1408.3+2626	2.100	20.22	0.52	
	Q6 Q1408.7+2665	1.928	18.74	0.22	
	Q7 FIRSTJ14162+2649	2.297	19.00	0.43	
	Q8 Q14144+256	1.800	20.50	0.18	
	Q9 Q14148+252	1.830	20.71	0.15	
	Q10 Q14149+251	1.917	18.86	0.22	
	Q11 2E1414+2513	1.057	19.50	0.46	
	Q12 1E14151+254	0.560	19.50	0.24	
	Q13 Q14151+254	2.310	19.57	0.35	
	Q14 HS1415+2701	2.500	17.70	0.46	
	Q15 2E1415+2557	0.237	17.20	0.80	
	Q16 2E1416+2523	0.674	18.70	-	
	Q17 HS1417+2547	2.200	18.10	0.52	
	Q18 KUV14189+2552	1.053	16.06	0.33	
	Q19 RXSJ14215+2408	0.084	17.27	0.30	
	Q20 PKS1423+24	0.649	17.26	0.36	
NGC5985					
0.008	Q1 = SBS1537+595	2.125	19.00	0.14	[52]
	Q2 SBS1535+596	1.968	18.66	0.29	
	Q3 HS1543+5921	0.807	17.63	0.28	
	Q4 SBS1532+598	0.690	17.57	0.19	
	Q5 SBS1549+590	0.348	17.42	0.21	
	Q6 SBS1533+588	1.895	18.39	0.19	
NGC6217	Q1 =				
0.005	1WGAJ1630.9+7810	0.358	20.60	-	[53]
	Q2 1WGAJ1634.4+7809	0.376	20.80	-	

Galaxy redshift	Quasar	Redshift Zo	Visual mag	B-V	*References*
IC4553 = 0.018	Arp 220				
	Q1 = 1WGAJ1533.8+2356	0.232	18.37	0.42	[54]
	Q2 Q1532+2332 (Arp9)	1.249	19.82	-	
	Q3 1WGAJ1535.0+2336	1.258	20.52	0.70	
	Q4 1WGAJ1537.2+2300	0.463	19.20	0.12	

Usually, the angular distances of our sample quasars from the respective parent galaxy are not more than 2 degrees**.** In some cases, large groups of quasars are reported in the vicinity of an active (usually Seyfert-type) galaxy (e.g. 63 quasars were reported in the vicinity of NGC450). Altogether, 225 quasars are sampled from 18 different galaxies. The low probability of some quasars being projected in the vicinity of a galaxy has been discussed many times by different authors, given in the references. Projected quasars (if any) are expected to show up by deviating from the rest of the sample, if general patterns are obtained.

3. Results

In this study, we follow the procedure described in Paper I.

Several crucial assumptions are taken:

- Quasars (Table 1) are spatially associated with the respective (parent) galaxy, i.e. all quasars of some galaxy are at about the same distance, as their parent galaxy. Therefore, all quasars in the vicinity of a low redshift (parent) galaxy should have the same cosmological redshift as this galaxy.
- Quasars are single bodies;
- Redshifts of quasars are taken to be composed by three components of different origin, according to Burbidge [55]:

$$(1 + z_o) = (1 + z_c) \cdot (1 + z_{gr}) \cdot (1 + z_d)\,, \tag{1}$$

where: z_o is the observed redshift, z_c is the cosmological redshift, z_{gr} is the intrinsic redshift, specified here as gravitational redshift, and z_d is the Doppler shift. The dominant component in a quasar redshift is the intrinsic redshift.

The intrinsic redshift is due to gravitational reddening and it is quantized, according to the Karlsson sequence.

All these assumptions are going to be checked with the results, obtained below. In Table1. to each group of quasars, associated with a galaxy, the cosmological redshift of this (parent) galaxy is attributed to all quasars of the respective group, i.e. $z_c = z_{gal}$ for all quasars of respective galaxy. Note that we assume here that the redshifts of all galaxies in this sample are entirely due to the expansion of the Universe. For the 18 galaxies of our sample this seems to be true, but in other cases one should be aware that also in redshifts of compact galaxies there could be a component of intrinsic (gravitational) origin. In the discussion below, we shall turn back to this point.

As a first step, all quasar redshifts are reduced with respect to the cosmological redshift-component of each quasar (i.e. to the cosmological redshift of respective parent galaxy):

$$z_i = (z_o - z_{gal}) / (1 + z_{gal}) \tag{2}$$

The z_i - shifts then contain the gravitational redshifts (dominant components) and the respective Doppler - shifts. For the gravitational redshift, we take for each z_i the nearest value from the Karlsson-sequence: 0.06, 0.30, 0.60, 0.96, 1.41, 1.96, 2.64, and so on. The discrepancy between the z_i - value and the corresponding nearest gravitational redshift z_{gr} from the Karlsson-sequence is attributed to the Doppler shift (e.g. velocity of ejection):

$$z_d = (z_i - z_{gr}) / (1 + z_{gr}) \tag{3}$$

In this way, each observed redshift is decomposed to the three components:

cosmological redshift (redshift of respective parent galaxy), the gravitational redshift, and the Doppler shift. The radii of the sample quasars are determined from:

$$\log(r_q/r_o) = \tfrac{1}{2} \log(L_q/L_o) + 2 \log(T_o/T_q), \tag{4}$$

where r, L, and T are radii, luminosities, and temperatures, respectively. Symbols q and o stay for quasar and Sun, respectively.

Temperatures of quasars are determined from their B - V (Table 1). For all quasars with unknown B – V the radii are determined from the M_q (absolute mag) versus r_q relation (Paper I):

$$M_q = 48.099 - 4.318 \log r_q . \tag{5}$$

We can further determine for each quasar the ratio r_{gr}/r_q, by substituting z_{gr} in the formula:

$$(1 + z_{gr}) = (1 - r_{gr}/r_q)^{-1/2}. \tag{6}$$

From this relation, the gravitational radius r_{gr} of each quasar can also be determined. For the gravitational radius holds:

$$r_{gr} = 2Gm_q/ c^2 . \tag{7}$$

With the r_{gr} already determined, we can now obtain the quasar masses m_q, and quasar densities ρ_q (G is the gravitational constant and c the velocity of light).

Physical characteristics of sample quasars are listed in Table 2.

Table 2. Physical characteristics of sample quasars. Columns are: 1 – ID of quasar, according to Table 1; 2 - observed redshift; 3 – gravitational redshift; 4 – Doppler shift; 5 – absolute magnitude; 6 – log r_q [cm]; 7 – log L_q [erg/s]; 8 – log m_q [g]; 9 – density ρ_q [g/cm^3]; 10 – reduced density [g/cm^3] to radius 8×10^{13} cm; 11 - ratio r_{gr}/r_q; 12 - quasar mass in units of 10^6 solar masses.

NGC450											
Q1	1.968	1.96	-0.003	-12.62	13.947	40.524	41.723	0.182	0.223	0.89	264.5
Q2	0.958	0.96	-0.007	-13.71	14.314	40.960	42.012	0.028	0.186	0.74	515
Q3	0.728	0.60	0.074	-12.66	14.071	40.540	41.685	0.071	0.154	0.61	242
Q4	0.956	0.96	-0.008	-13.91	14.361	41.040	42.059	0.023	0.188	0.74	570
Q5	1.893	1.96	-0.028	-12.06	13.932	40.300	41.708	0.195	0.223	0.89	255.5
Q6	0.070	0.06	0.004	-12.61	14.060	40.520	40.930	0.013	0.027	0.11	42.6
Q7	0.468	0.60	-0.088	-12.13	13.694	40.328	41.308	0.402	0.153	0.61	101.5
Q8	1.424	1.41	0.0	-12.28	14.174	40.388	41.921	0.060	0.208	0.83	416.5
Q9	2.005	1.96	0.009	-13.26	14.210	40.780	41.986	0.054	0.222	0.89	484.5
Q10	1.240	1.41	-0.076	-13.41	14.245	40.840	41.992	0.043	0.208	0.83	490.5
Q11	1.302	1.41	-0.051	-11.91	13.897	40.240	41.644	0.214	0.209	0.83	220.5
Q12	1.003	0.96	0.016	-12.84	14.053	40.612	41.751	0.093	0.186	0.74	281.5
Q13	1.758	1.96	-0.074	-13.14	14.113	40.732	41.889	0.085	0.224	0.89	387.5
Q14	1.896	1.96	-0.027	-12.22	13.879	40.364	41.655	0.249	0.223	0.89	226
Q15	1.102	0.96	0.066	-14.21	14.430	41.160	42.128	0.016	0.181	0.74	670
Q16	0.238	0.30	-0.053	-13.66	14.243	40.940	41.682	0.022	0.105	0.41	240.5
Q17	0.910	0.96	-0.031	-11.43	13.709	40.048	41.407	0.455	0.186	0.74	130
Q18	0.976	0.96	0.002	-12.96	14.141	40.660	41.839	0.062	0.184	0.74	345
Q19	1.235	1.41	-0.078	-13.81	14.337	41.000	42.084	0.028	0.206	0.83	605
Q20	0.412	0.30	0.080	-12.45	14.014	40.456	41.454	0.062	0.103	0.41	142.2
Q21	0.935	0.96	-0.019	-11.81	13.874	40.200	41.572	0.213	0.187	0.74	186.5
Q22	0.995	0.96	0.012	-12.88	13.598	39.649	41.296	0.759	0.186	0.74	99
Q23	0.181	0.06	0.108	-12.58	14.303	40.508	41.174	0.004	0.025	0.11	74.5
Q24	0.350	0.30	0.032	-12.49	14.063	40.472	41.503	0.049	0.103	0.41	159.2
Q25	1.908	1.96	-0.023	-12.06	13.932	40.300	41.708	0.195	0.223	0.89	255.5
Q26	1.365	1.41	-0.024	-14.01	14.384	41.080	42.131	0.023	0.210	0.83	675
Q27	1.585	1.41	0.066	-11.62	13.735	40.124	41.482	0.451	0.209	0.83	151.8
Q28	1.279	1.41	-0.060	-12.32	14.067	40.404	41.814	0.098	0.210	0.83	326
Q29	1.968	1.96	-0.003	-11.93	13.797	40.248	41.574	0.363	0.223	0.89	187.5
Q30	2.055	1.96	0.026	-11.91	13.897	40.240	41.674	0.229	0.223	0.89	236
Q31	1.263	1.41	-0.066	-12.55	14.103	40.496	41.850	0.083	0.209	0.83	354
Q32	1.316	1.41	-0.045	-12.57	14.098	40.504	41.845	0.085	0.209	0.83	349.7
Q33	2.190	1.96	0.071	-13.19	14.073	40.752	41.849	0.102	0.223	0.89	353.5
Q34	2.050	1.96	0.024	-12.81	14.106	40.600	41.882	0.088	0.224	0.89	381
Q35	1.052	0.96	0.041	-12.91	14.138	40.640	41.836	0.063	0.186	0.74	342.5
Q36	0.090	0.06	0.022	-14.16	14.501	41.140	41.371	0.002	0.031	0.11	117.5
Q37	2.019	1.96	0.014	-11.71	13.851	40.160	41.627	0.283	0.223	0.89	212
Q38	0.649	0.60	0.024	-12.21	13.819	40.360	41.433	0.226	0.153	0.61	135.5
Q39	0.960	0.96	-0.006	-13.61	14.291	40.920	41.989	0.031	0.185	0.74	487.5
Q40	0.202	0.30	-0.081	-12.38	14.311	40.428	41.751	0.016	0.105	0.41	281.5
Q41	0.078	0.06	0.011	-12.06	13.932	40.300	40.802	0.024	0.027	0.11	31.8
Q42	1.445	1.41	0.008	-13.16	14.187	40.740	41.934	0.056	0.207	0.83	429.3
Q43	1.911	1.96	-0.022	-12.06	13.932	40.300	41.708	0.195	0.223	0.89	255.5
Q44	1.165	0.96	0.098	-13.06	14.164	40.700	41.862	0.056	0.186	0.74	363.6
Q45	2.112	1.96	0.045	-12.51	14.036	40.480	41.813	0.121	0.223	0.89	325
Q46	0.328	0.30	0.015	-12.40	13.991	40.436	41.430	0.069	0.103	0.41	134.7

Table 2 continued

Q47	0.135	0.06	0.064	-12.76	14.094	40.580	40.965	0.011	0.027	0.11	46.1
Q48	1.943	1.96	-0.012	-12.21	13.853	40.360	41.630	0.280	0.223	0.89	213.1
Q49	0.909	0.96	-0.032	-12.30	14.063	40.396	41.761	0.089	0.186	0.74	288.5
Q50	1.073	0.96	0.052	-12.96	14.141	40.660	41.839	0.062	0.185	0.74	344.8
Q51	1.355	1.41	-0.029	-12.50	14.177	40.476	41.924	0.059	0.208	0.83	419.5
Q52	0.438	0.30	0.099	-13.41	14.245	40.840	41.685	0.021	0.101	0.41	241.9
Q53	0.772	0.60	0.101	-12.26	13.978	40.380	41.592	0.108	0.153	0.61	195.6
Q54	1.310	1.41	-0.047	-11.91	13.897	40.240	41.644	0.214	0.208	0.83	220.4
Q55	1.555	1.41	0.054	-12.47	14.059	40.464	41.806	0.102	0.209	0.83	319.8
Q56	2.252	1.96	0.092	-12.21	13.967	40.360	41.743	0.166	0.223	0.89	277
Q57	2.043	1.96	0.022	-12.01	13.921	40.280	41.697	0.206	0.223	0.89	249
Q58	0.988	0.96	0.008	-12.46	14.025	40.460	41.723	0.106	0.186	0.74	264.1
Q59	2.022	1.96	0.015	-12.01	13.921	40.280	41.697	0.206	0.223	0.89	249
Q60	1.889	1.96	-0.030	-12.51	14.036	40.480	41.813	0.121	0.223	0.89	325
Q61	1.763	1.96	-0.072	-12.61	14.007	40.520	41.783	0.138	0.222	0.89	303.3
Q62	1.930	1.96	-0.016	-13.11	14.175	40.720	41.952	0.064	0.224	0.89	447.3
Q63	0.355	0.30	0.036	-14.16	14.418	41.140	41.858	0.010	0.107	0.41	360.9
					NGC613						
Q1	2.222	1.96	0.083	-10.32	13.529	39.604	41.305	1.247	0.223	0.89	101
Q2	2.059	1.96	0.028	-10.09	13.476	39.512	41.252	1.593	0.223	0.89	89.5
Q3	2.062	1.96	0.029	-10.40	13.548	39.636	41.324	1.145	0.223	0.89	105.5
Q4	1.855	1.96	-0.041	-10.11	13.481	39.520	41.257	1.560	0.223	0.89	90.5
Q5	1.413	1.41	-0.004	-9.91	13.434	39.440	41.181	1.804	0.208	0.83	76
Q6	1.482	1.41	0.025	-10.10	13.478	39.516	41.225	1.473	0.208	0.83	84
					NGC622						
Q1	0.910	0.96	-0.042	-15.79	14.714	41.792	42.412	0.004	0.167	0.74	1290
Q2	1.460	1.41	0.004	-15.02	14.415	41.484	42.162	0.020	0.212	0.83	726.5
					NGC1068						
Q1	0.261	0.30	-0.033	-14.15	14.367	41.136	41.807	0.012	0.102	0.41	320.8
Q2	0.468	0.60	-0.085	-10.56	13.572	39.700	41.186	0.705	0.153	0.61	76.7
Q3	0.726	0.60	0.076	-11.11	13.621	39.920	41.235	0.561	0.153	0.61	86
Q4	0.649	0.60	0.028	-10.91	13.495	39.840	41.109	1.005	0.153	0.61	64.2
Q5	1.054	0.96	0.045	-10.71	13.680	39.760	41.378	0.521	0.186	0.74	119.3
Q6	1.552	1.41	0.056	-11.16	13.704	39.940	41.451	0.521	0.208	0.83	141.3
Q7	1.112	0.96	0.074	-10.93	13.308	39.848	41.006	2.883	0.186	0.74	50.7
Q8	0.385	0.30	0.062	-9.96	13.538	39.460	40.978	0.552	0.103	0.41	47.5
Q9	2.018	1.96	0.017	-11.18	13.747	39.948	41.523	0.458	0.223	0.89	166.8
Q10	0.684	0.60	0.049	-10.71	13.518	39.760	41.132	0.901	0.153	0.61	67.8
Q11	0.655	0.60	0.031	-10.72	13.412	39.764	41.026	1.471	0.153	0.61	53.1
Q12	0.630	0.60	0.016	-9.30	13.045	39.196	40.659	7.961	0.153	0.61	22.8
Q13	1.139	0.96	0.088	-11.19	13.812	39.952	41.510	0.282	0.186	0.74	162
Q14	1.292	1.41	-0.052	-10.88	13.819	39.828	41.566	0.306	0.208	0.83	184.1
Q15	1.815	1.96	-0.052	-11.00	13.600	39.876	41.376	0.900	0.223	0.89	118.9
Q16	2.315	2.64	-0.092	-9.47	13.305	39.264	41.100	3.653	0.233	0.92	62.9
					NGC1073						
Q1	0.601	0.60	-0.003	-11.91	13.897	40.240	41.511	0.157	0.153	0.61	162.3
Q2	1.400	1.41	-0.008	-10.61	13.596	39.720	41.343	0.855	0.208	0.83	110
Q3	1.941	1.96	-0.010	-11.31	13.758	40.000	41.535	0.434	0.223	0.89	171
Q4	0.546	0.60	-0.038	-11.73	13.674	40.168	41.288	0.441	0.153	0.61	97

					NGC1097						
Q2	2.143	1.96	0.057	-10.58	13.589	39.708	41.366	0.945	0.223	0.89	116.1
Q3	2.265	1.96	0.099	-11.88	13.890	40.228	41.667	0.236	0.223	0.89	232.1
Q6	2.034	1.96	0.021	-10.68	13.613	39.748	41.389	0.849	0.223	0.89	122.4
Q7	0.374	0.30	0.053	-11.68	13.844	40.148	41.284	0.135	0.103	0.41	96.2
Q9	1.588	1.41	0.070	-10.28	13.520	39.588	41.267	1.216	0.208	0.83	92.4
Q10	0.359	0.30	0.042	-10.68	13.613	39.748	41.052	0.391	0.103	0.41	56.4
Q12	0.874	0.96	-0.047	-11.08	13.705	39.908	41.403	0.463	0.186	0.74	126.5
Q13	1.985	1.96	0.004	-10.58	13.589	39.708	41.366	0.945	0.223	0.89	116.1
Q14	1.045	0.96	0.039	-11.38	13.775	40.028	41.473	0.336	0.186	0.74	148.5
Q15	2.269	1.96	0.100	-10.28	13.520	39.588	41.296	1.301	0.223	0.89	98.9
Q16	0.783	0.60	0.110	-10.58	13.589	39.708	41.203	0.650	0.153	0.61	79.9
Q18	1.577	1.41	0.065	-9.98	13.450	39.468	41.197	1.674	0.208	0.83	78.8
Q19	2.063	1.96	0.031	-10.08	13.474	39.508	41.250	1.611	0.223	0.89	88.9
Q20	0.088	0.06	0.023	-10.18	13.497	39.548	40.367	0.180	0.028	0.11	11.6
Q21	1.875	1.96	-0.032	-11.68	13.844	40.148	41.620	0.292	0.223	0.89	208.7
Q23	1.000	0.96	0.016	-12.68	14.076	40.548	41.774	0.084	0.186	0.74	296.9
Q24	0.340	0.30	0.027	-11.98	13.914	40.268	41.353	0.098	0.103	0.41	112.9
Q25	1.100	0.96	0.067	-9.68	13.381	39.348	41.079	2.060	0.186	0.74	60
Q26	0.887	0.96	-0.041	-10.18	13.497	39.548	41.195	1.209	0.186	0.74	78.3
					NGC2639						
Q1	1.177	0.96	0.098	-14.12	14.348	41.124	42.046	0.024	0.186	0.74	556
Q2	1.105	0.96	0.062	-13.02	14.197	40.684	41.895	0.048	0.186	0.74	393
Q3	1.522	1.41	0.035	-12.75	14.115	40.576	41.862	0.079	0.210	0.83	363.7
Q4	0.780	0.60	0.101	-13.31	14.372	40.800	41.986	0.018	0.156	0.61	483.7
Q5	1.494	1.41	0.024	-14.26	14.612	41.180	42.359	0.008	0.210	0.83	1143
Q7	2.000	1.96	0.002	-12.81	14.165	40.600	41.941	0.067	0.224	0.89	436.6
Q8	2.800	2.64	0.033	-13.18	14.192	40.748	41.987	0.062	0.234	0.92	484.7
Q10	0.305	0.30	-0.007	-14.38	14.311	41.228	41.751	0.016	0.105	0.41	281.8
Q14	2.124	1.96	0.044	-13.44	14.234	40.852	42.011	0.048	0.221	0.89	512.5
Q15	1.525	1.41	0.037	-13.40	14.115	40.836	41.862	0.078	0.207	0.83	363.9
Q16	0.323	0.30	0.007	-13.78	14.133	40.988	41.573	0.036	0.104	0.41	187
					NGC3034=M82						
Q1	1.010	0.96	0.024	-8.39	13.271	38.832	40.969	3.423	0.186	0.74	46.5
Q2	2.048	1.96	0.029	-8.33	13.203	38.808	40.980	5.590	0.223	0.89	47.7
Q3	2.054	1.96	0.031	-7.50	12.936	38.476	40.712	19.147	0.223	0.89	25.8
Q4	0.85	0.96	-0.057	-7.71	13.411	38.560	41.109	1.796	0.186	0.74	64.3
Q5	2.040	1.96	0.026	-7.52	12.868	38.484	40.644	26.202	0.223	0.89	22
Q6	2.240	1.96	0.094	-6.43	12.628	38.048	40.457	89.168	0.252	0.89	14.3
Q7	0.930	0.96	-0.016	-8.45	13.561	38.856	41.259	0.899	0.186	0.74	90.8
Q8	0.960	0.96	-0.001	-8.79	13.982	38.992	41.680	0.129	0.185	0.74	239.2
Q9	0.740	0.60	0.086	-5.83	12.489	37.808	40.103	103.04	0.153	0.61	6.3
Q10	0.675	0.60	0.046	-8.03	12.999	38.688	40.613	9.863	0.153	0.61	20.5
Q11	0.626	0.60	0.015	-8.93	13.207	39.048	40.821	3.777	0.153	0.61	33.1
Q12	1.086	0.96	0.063	-9.84	13.533	39.412	41.231	1.024	0.186	0.74	85.1
					NGC3079						
Q1	1.410	1.41	-0.004	-11.83	13.743	40.208	41.490	0.435	0.208	0.83	154.5
Q2	0.898	0.96	-0.036	-12.39	14.062	40.432	41.760	0.090	0.187	0.74	287.7
Q3	1.021	0.96	0.027	-12.60	14.213	40.516	41.911	0.045	0.187	0.74	407.3
Q4	0.215	0.30	-0.069	-10.91	13.996	39.840	41.436	0.067	0.103	0.41	136.5

Table 2 continued

Q5	1.037	0.96	0.035	-10.29	13.836	39.592	41.534	0.253	0.186	0.74	171
Q6	1.530	1.41	0.046	-11.24	13.804	39.972	41.550	0.329	0.208	0.83	177.6
Q7	0.072	0.06	0.008	-13.00	14.150	40.676	41.020	0.009	0.028	0.11	52.4
Q8	2.102	1.96	0.044	-12.68	14.076	40.548	41.852	0.101	0.224	0.89	355.6
Q9	1.413	1.41	-0.003	-13.33	14.089	40.808	41.836	0.088	0.207	0.83	342.7
Q10	1.415	1.41	-0.002	-13.33	14.089	40.808	41.836	0.088	0.207	0.83	342.7
Q11	1.154	0.96	0.094	-7.25	12.818	38.376	40.516	27.507	0.186	0.74	16.4
Q12	0.352	0.30	0.036	-9.14	13.256	39.132	40.696	2.023	0.103	0.41	24.8
Q13	1.760	1.96	-0.071	-14.23	14.357	41.168	42.133	0.028	0.226	0.89	679
Q14	1.154	0.96	0.094	-11.90	13.993	40.236	41.691	0.123	0.186	0.74	245.5
Q15	0.219	0.30	-0.066	-9.08	13.242	39.108	40.682	2.156	0.103	0.41	24
Q16	3.216	3.47	-0.061	-10.20	13.501	39.556	41.308	1.520	0.239	0.95	101.6
					NGC3628						
Q1	1.413	1.41	-0.002	-11.24	13.733	39.972	41.480	0.456	0.208	0.83	151
Q2	2.060	1.96	0.031	-11.39	13.763	40.032	41.539	0.425	0.223	0.89	173
Q3	1.750	1.96	-0.074	-10.72	13.532	39.764	41.308	1.231	0.223	0.89	101.7
Q4	2.150	1.96	0.061	-10.86	13.696	39.820	41.472	0.579	0.223	0.89	148.3
Q8	2.430	2.64	-0.060	-9.33	13.325	39.208	41.120	3.325	0.233	0.92	66
Q9	1.940	1.96	-0.010	-11.24	13.733	39.972	41.509	0.488	0.223	0.89	161.6
Q10	2.490	2.64	-0.044	-9.60	13.362	39.316	41.157	2.804	0.233	0.92	72
Q11	2.370	2.64	-0.077	-10.25	13.751	39.576	41.546	0.468	0.232	0.92	175.8
Q12	2.100	1.96	0.044	-10.18	13.290	39.548	41.066	3.755	0.223	0.89	58.2
Q13	2.140	1.96	0.058	-10.28	13.816	39.588	41.592	0.332	0.223	0.89	195.7
Q14	1.740	1.96	-0.077	-10.21	13.370	39.560	41.146	2.594	0.223	0.89	70.1
Q15	2.320	2.64	-0.091	-12.45	14.325	40.456	42.120	0.033	0.230	0.92	658.7
Q16	0.060	0.06	-0.003	-10.10	13.478	39.516	40.349	0.196	0.028	0.11	11.2
Q17	2.540	2.64	-0.030	-10.28	13.528	39.588	41.323	1.308	0.233	0.92	105.2
Q18	2.380	2.64	-0.074	-10.73	13.618	39.768	41.413	0.864	0.233	0.92	129.4
Q19	2.110	1.96	0.048	-9.33	13.232	39.208	41.008	4.909	0.223	0.89	50.9
Q20	3.009	2.64	0.098	-10.47	13.659	39.664	41.454	0.716	0.233	0.92	142.2
					NGC4235						
Q1	0.334	0.30	0.019	-15.65	14.764	41.736	42.203	0.002	0.105	0.41	798.5
Q2	0.137	0.06	0.065	-15.30	14.682	41.596	41.553	0.0008	0.029	0.11	178.6
					NGC4258						
Q1	0.398	0.30	0.073	-8.97	13.217	39.064	40.657	2.416	0.103	0.41	22.7
Q2	0.654	0.60	0.032	-9.42	13.261	39.244	40.875	2.950	0.153	0.61	37.5
					NGC4410						
Q1	2.237	1.96	0.067	-15.61	14.619	41.720	42.395	0.008	0.216	0.89	1243
Q2	0.662	0.60	0.013	-15.94	14.456	41.852	42.070	0.012	0.153	0.61	587
Q3	1.903	1.96	-0.043	-15.61	14.546	41.720	42.322	0.012	0.231	0.89	1049
Q5	0.535	0.60	-0.064	-17.89	14.361	41.632	41.974	0.019	0.156	0.61	471.4
Q6	1.776	1.96	-0.085	-15.79	14.486	41.792	42.262	0.015	0.220	0.89	914.5
Q8	0.085	0.06	-0.001	-18.54	14.821	41.892	41.691	0.0004	0.027	0.11	245.7
Q9	1.590	1.41	0.049	-15.15	14.707	41.536	42.454	0.005	0.203	0.83	1421.5
Q10	1.502	1.41	0.013	-16.36	14.757	42.020	42.504	0.004	0.204	0.83	1594.5
Q11	0.628	0.60	-0.008	-15.85	14.483	41.816	42.096	0.011	0.159	0.61	624
Q12	1.043	0.96	0.017	-16.44	14.825	42.052	42.523	0.003	0.210	0.74	1668.5
Q13	1.363	1.41	-0.044	-15.94	14.762	41.852	42.509	0.004	0.209	0.83	1615
Q15	1.471	1.41	0.0	-17.59	14.555	41.512	42.302	0.010	0.202	0.83	1003

Table 2 continued

Q16	1.076	0.96	0.033	-15.70	14.563	41.756	42.261	0.009	0.188	0.74	912
Q17	1.345	1.41	-0.051	-15.86	14.632	41.820	42.378	0.007	0.201	0.83	1195
Q18	1.090	0.96	0.040	-16.06	14.786	41.900	42.484	0.003	0.175	0.74	1525
Q19	1.715	1.41	0.099	-15.69	14.406	41.752	42.153	0.021	0.213	0.83	711
Q20	0.681	0.60	0.025	-17.44	14.756	42.452	42.370	0.003	0.152	0.61	1171.5
Q21	2.649	2.64	-0.022	-15.10	14.585	41.516	42.380	0.010	0.231	0.92	1199
Q22	0.773	0.60	0.081	-16.40	14.635	42.036	42.248	0.005	0.145	0.61	885.5
Q23	0.064	0.06	-0.021	-17.46	15.327	42.460	42.197	.00004	0.028	0.11	787
Q24	0.398	0.30	0.049	-16.60	14.633	42.116	42.072	0.004	0.115	0.41	590.5
Q25	1.429	1.41	-0.017	-16.14	14.713	41.932	42.460	0.005	0.208	0.83	1440.5
						NGC4579					
Q2	0.662	0.60	0.034	-11.61	13.619	40.120	41.233	0.566	0.153	0.61	85.5
						NGC5548					
Q1	0.852	0.96	-0.071	-15.23	14.666	41.568	42.364	0.006	0.202	0.74	1156.5
Q2	0.184	0.06	0.098	-15.60	14.676	41.716	41.546	0.0008	0.028	0.11	175.8
Q3	0.727	0.60	0.061	-14.73	14.550	41.368	42.164	0.008	0.158	0.61	730
Q4	2.425	2.64	-0.075	-14.55	14.321	41.296	42.116	0.034	0.233	0.92	653.5
Q5	2.100	1.96	0.030	-13.41	14.416	40.840	42.192	0.021	0.223	0.89	778.5
Q6	1.928	1.96	-0.027	-14.89	14.413	41.432	42.189	0.021	0.220	0.89	773.5
Q7	2.297	1.96	0.095	-14.63	14.587	41.328	42.363	0.0095	0.222	0.89	1154.5
Q8	1.800	1.96	-0.070	-13.13	14.014	40.728	41.790	0.134	0.223	0.89	308.5
Q9	1.830	1.96	-0.060	-12.92	13.938	40.644	41.715	0.189	0.222	0.89	259.3
Q10	1.917	1.96	-0.031	-14.77	14.389	41.384	42.165	0.024	0.225	0.89	732
Q11	1.057	0.96	0.032	-14.13	14.511	41.128	42.209	0.011	0.181	0.74	809
Q12	0.560	0.60	-0.041	-14.13	14.286	41.128	41.899	0.026	0.151	0.61	396.6
Q13	2.310	1.96	0.100	-14.06	14.396	41.100	42.173	0.023	0.223	0.89	744
Q14	2.500	2.64	-0.055	-15.93	14.871	41.848	42.666	0.003	0.259	0.92	2316.5
Q15	0.237	0.30	-0.065	-16.43	15.232	42.048	42.672	0.0002	0.091	0.41	2347
Q16	0.674	0.60	0.029	-14.93	14.597	41.448	42.211	0.006	0.146	0.61	812
Q17	2.200	1.96	0.063	-15.53	14.841	41.688	42.617	0.003	0.225	0.89	2069.5
Q18	1.053	0.96	0.030	-17.57	15.079	42.504	42.777	0.0008	0.180	0.74	2992
Q19	0.084	0.06	0.006	-16.36	14.809	42.020	41.680	0.0004	0.026	0.11	239.2
Q20	0.649	0.60	0.013	-16.37	14.868	42.024	42.481	0.002	0.170	0.61	1514.5
						NGC5985					
Q1	2.125	1.96	0.047	-12.62	13.868	40.524	41.644	0.263	0.223	0.89	220.2
Q2	1.968	1.96	-0.005	-12.96	14.116	40.660	41.892	0.084	0.224	0.89	390.2
Q3	0.807	0.96	-0.085	-13.99	14.309	41.072	42.007	0.029	0.188	0.74	507.8
Q4	0.690	0.60	0.048	-14.05	14.210	41.096	41.823	0.037	0.152	0.61	332.9
Q5	0.348	0.30	0.028	-14.20	14.263	41.156	41.703	0.020	0.105	0.41	252.4
Q6	1.895	1.96	-0.030	-13.23	14.046	40.768	41.822	0.116	0.224	0.89	331.8
						NGC6217					
Q1	0.358	0.30	0.039	-10.08	13.474	39.508	40.913	0.742	0.103	0.41	41
Q2	0.376	0.30	0.053	-9.88	13.427	39.428	40.867	0.919	0.103	0.41	36.8
						IC4553					
Q1	0.232	0.30	-0.069	-15.01	14.655	41.480	42.095	0.003	0.102	0.41	622.5
Q2	1.249	1.41	-0.083	-13.56	14.280	40.900	42.026	0.037	0.209	0.83	531.5
Q3	1.258	1.41	-0.080	-12.86	14.442	40.620	42.189	0.017	0.203	0.83	772.5
Q4	0.463	0.30	0.105	-14.18	14.149	41.148	41.588	0.033	0.102	0.41	193.9

Clearly, the gravitational redshift should depend on the density of the quasar. In fact, the relation "density-gravitational redshift" includes also the inverse square of the quasar radius, as shown in Paper I:

$$\rho_q = (3/4\pi) \cdot (c^2/2G) \cdot (1/r_q^2) \cdot \{1 - 1/(1 + z_{gr}).^2\} \qquad (8)$$

From eq.(8), we can reduce all densities to some radius of choice, in order to avoid the dependence of density on radius. In Table 2, column 10, the reduced densities to a radius 8×10^{13} cm are listed (the choice of radius is arbitrary). Fig (1) shows the plot of reduced densities versus observed redshifts. The sample of 225 quasars fits well the theoretical (dashed) line for a radius 8×10^{13} cm. We believe, this is strong evidence that all premises assumed were true. There are several quasars, which deviate from the general sequence in Fig (1) (marked by numbers).

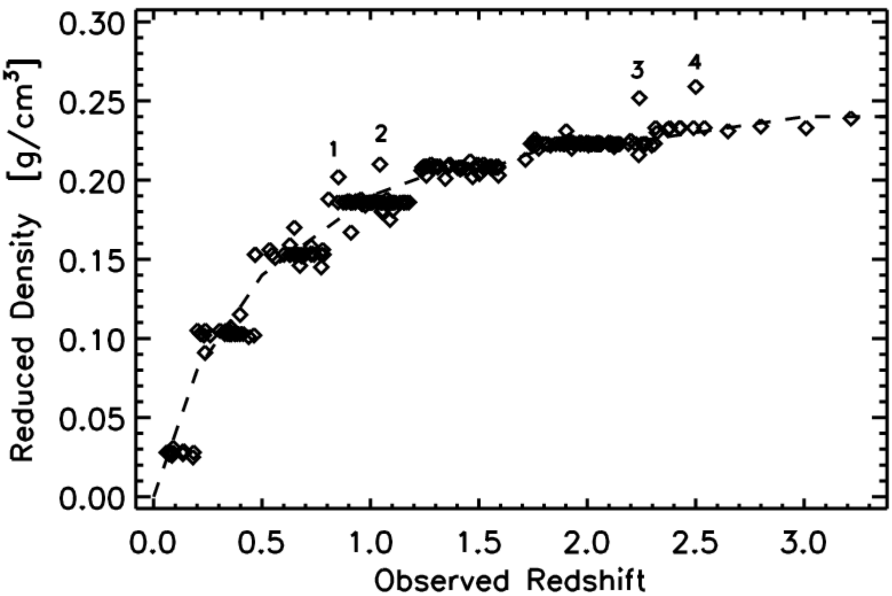

Figure 1. Diagram "Reduced density – observed redshift" for 225 local quasars. All densities are reduced to a radius of 8×10^{13} cm. The dashed line is the theoretical line from eq (8) for radius 8×10^{13} cm. The numbered QSOs are: 1 = NGC5548Q1, 2 = NGC4410Q12, 3 = M82Q6, 4 = NGC5548Q14

Several causes could contribute to the scatter on this diagram: observational errors, variability of the QSOs, the use of the "absolute mag – radius"relation to determine the radii of quasars with unknown B-V, or a projection of a more distant quasar. Another cause for scatter could also be the redshift of the parent galaxy, if some intrinsic (gravitational reddening) component is present in the galaxy-redshift. A careful examination of all these causes goes, however, beyond the scope of this paper.

The relation "density – redshift" needs an explanation. As in Paper I, we believe that this relation shows possibly an evolutionary effect: the redshift of a quasar (actually, it is only its gravitational component) decreases as its density drops. The physical processes behind this evolution are not yet clear. If density decreases, however, disintegration processes of matter are probably involved.

If disintegration processes are involved, the quasar radius in the course of evolution should increase. It could be calculated that a quasar with $z_{gr} = 3.22$ and reduced density = 0.239 will "travel" along the diagram with increasing radius, and will reach position $z_{gr} = 0.07$, and reduced density = 0.03 when the radius is increased 8 times with respect to the initial position.

Let us remind the reader that Ambartsumian [56] put forward a radically new hypothesis, according to which the unusual activity in active galactic nuclei is due to the disintegration of matter of yet unknown origin and properties. There is an interesting consequence of eq.(8), already discussed in Paper I. At large redshifts, the evolution of redshift to lower values as density decreases is very fast. This could explain why very large values of QSOs - redshifts have not been observed. The well known problem of declining number of quasars with redshifts $z > 3$ is also explained in a natural way. In a number of papers, Halton Arp [28, 36, 37] suggested an evolutionary scenario for quasars, where quasar redshifts decrease when receding from the parent galaxy (ejection hypothesis). The end-products of the evolution of quasars, according to Arp's scenario, are galaxies. Thus this evolution could be detected by the increasing luminosity (and radius) of the quasar in the course of its evolution.

We shall test first the Arp's hypothesis with the quasars of NGC450 (63 quasars).

In Fig (2), the absolute magnitudes are plotted against the observed redshifts for these quasars (upper panel). A trend of increasing absolute mag with decreasing redshift could possibly exist. We could try to improve the evolutionary picture in the following way. In Paper I, it has been shown that a relation "absolute magnitude – mass" exists for quasars:

$$M_q = 158.808 - 4.107 \cdot \log m_q \qquad (9)$$

As quasars do have different masses, the evolutionary effect in the upper panel of Fig (2) could be masked by this "absolute mag. – mass" relation. In order to eliminate the influence of different masses, all quasar magnitudes were reduced to a single mass (a mass of choice), $m_q = 5.3 \times 10^{41}$ g. Clearly, the choice of this mass is arbitrary and should not have influence on the conclusions. The result is shown in the middle panel of Fig (2) and the evolutionary increase of absolute magnitude, corresponding to a decreasing redshift is now obvious. In the lower panel of Fig (2), the corresponding increase is shown of the quasar radii. As expected, at least one part of the brightness increase is due to the increase of the quasar radius. The same procedure was repeated with the groups of quasars of M82 (mags reduced to a mass of 6.6×10^{40} g), NGC1068, NGC1097, and NGC3628 (all mags reduced to a mass of 2.4×10^{41} g), NGC2639 and NGC3079 (mags reduced to a mass of 7.3×10^{41} g), and NGC4410 and NGC5548 (mags reduced to a mass of 1.6×10^{42} g).

Table 3. Coefficients for eq. (10), fitting the curves on Fig. 2, middle panel and on Fig. 3.

Quasars of galaxy	K1	K2	K3
NGC 450	-18.0007903	-72.4023860	6.201239506
NGC4410 and NGC5548	-19.5467805	-34.4308619	2.509362351
NGC2639 and NGC3079	-23.1655734	-311.797871	24.85949595
NGC1068, NGC1097, and NGC3628	-15.3563492	-37.4438895	3.757783143

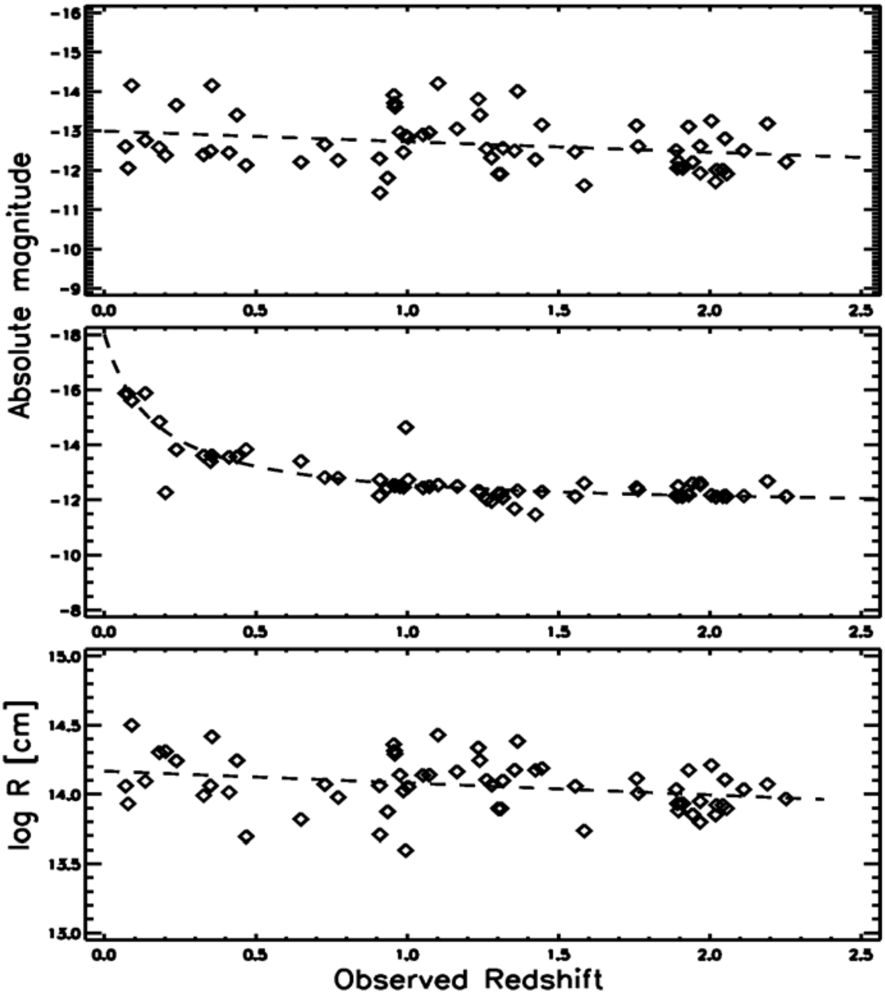

Figure 2. (upper panel). Relation of absolute magnitude with observed redshift for 63 quasars of NGC450 (data from Table 2). Note the trend of increasing mag with decreasing redshift; (middle panel) The same relation for the same 63 quasars of NGC450 with all magnitudes reduced to a mass of 5.3×10^{41} g (see text); (lower panel) Relation of quasar radius versus observed redshift for the same 63 quasars of NGC 450.

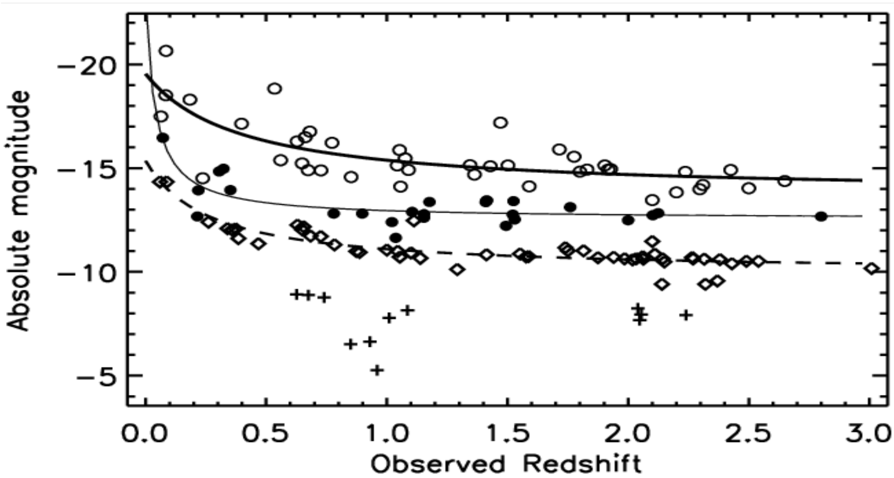

Figure 3. Relation of absolute magnitude with observed redshift for quasars of: M82 (crosses), all mags are reduced to a mass of 6.6×10^{40} g; NGC1068, NGC1097, and NGC3628 (rhombs), all mags are reduced to a mass of 2.4×10^{41} g; NGC2639 and NGC3079 (dots), all mags are reduced to a mass of 7.3×10^{41} g; NGC4410 and NGC5548 (circles), all mags are reduced to a mass of 1.6×10^{42} g The fitting functions are from eq. (10) and Table 3 (see text).

The results are shown in Fig (3). With exception of the M82 quasars (which are least luminous), the rest of the data shows clear increase of absolute magnitude with decreasing redshift. This is strong evidence in favor of Arp's scenario. The separation of quasars of different galaxies in different groups is necessary, because quasars of different galaxies seem to show intrinsic differences in their luminosities and radii (Paper I). From Fig (3), apparently the least luminous quasars are quasars of M82, and the most luminous are the quasars of NGC4410 and NGC5548. The reason for this separation is not yet clear. Combining the evidence of Fig (2) and Fig (3), the evolutionary increase in luminosity, as predicted by the Arp's scenario, seems to be confirmed. The lines drown in Fig (2), middle panel, and in Fig (3) correspond to the function:

$$M_q = (k_1 + k_2.\ z_o)/(1 + k_3.z_o) \qquad (10)$$

and which is fitted to the different curves with different coefficients. These are listed in Table 3. The physical meaning of these coefficients is not yet clear. Moreover, the fitting function (10) could be an approximation to another, yet unknown (true) relation.

In Fig (4), the relation is shown between the absolute magnitude and the radius for sample quasars and for stars (data from Table 2). The mean line for quasars (correlation coeff.: -0.95) is defined by:

$$M_q = 50.65 - 4.51 \cdot \log r_q \qquad (11)$$

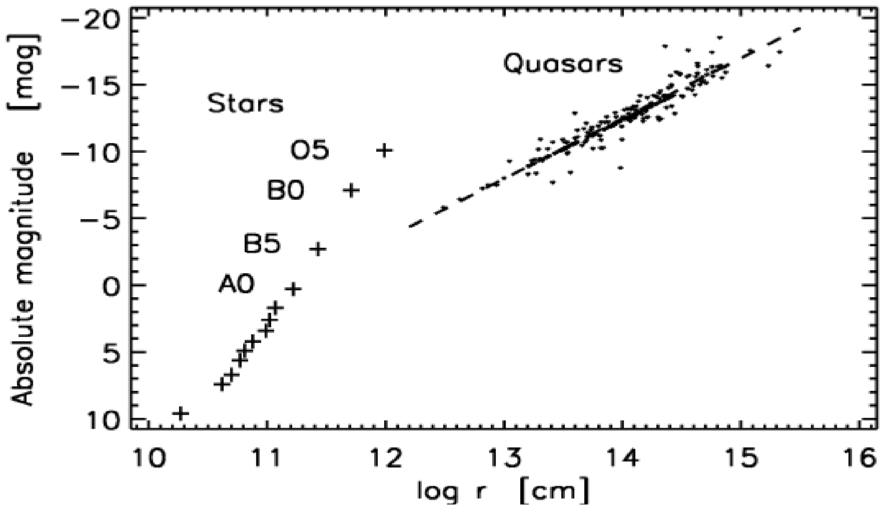

Figure 4. Diagram "absolute magnitude - radius" for 225 local quasars (dots). The same relationship is shown also for stars (crosses), as mean values for O5, B0, B5,.,M5.

Thus respective relation from Paper I is confirmed.

In Fig (5), the absolute magnitude is plotted versus the mass for the sample quasars and also for stars (data from Table 2). The mean line for quasars (correlation co-eff.:-0.85) is defined by:

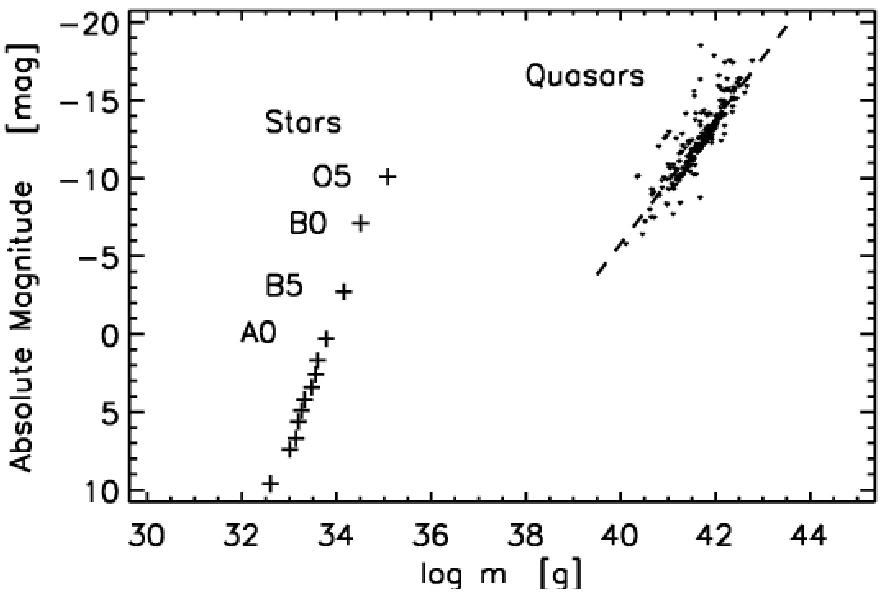

Figure 5. Diagram "absolute magnitude - mass" for 225 local quasars (dots). The same relationship is shown also for stars (crosses), as mean values for: O5, B0, B5,.,M5.

$$M_q = 153.31 - 3.98 \cdot \log m_q \quad (12)$$

Thus respective relation from Paper I is confirmed.

The “mass-radius” relation is shown in Fig (6) (data from Table 2), for the sample quasars (correlation coeff.: 0.90) and for stars. The mean line for quasars is:

$$\log m_q = 28.82 + 0.92 \cdot \log r_q \quad (13)$$

The respective relation from Paper I is confirmed.

This relation implies that fainter quasars have larger gravitational redshifts, which has been discussed already by Greenstein and Schmidt [30].

The “mass-luminosity” relation (data from Table 2.) is shown in Fig (7) for the sample quasars (correlation coeff: 0.87) and for stars. The mean line for quasars is:

$$\log L_q = -25.31 + 1.58 \cdot \log m_q \quad (14)$$

The respective relation from Paper I is confirmed.

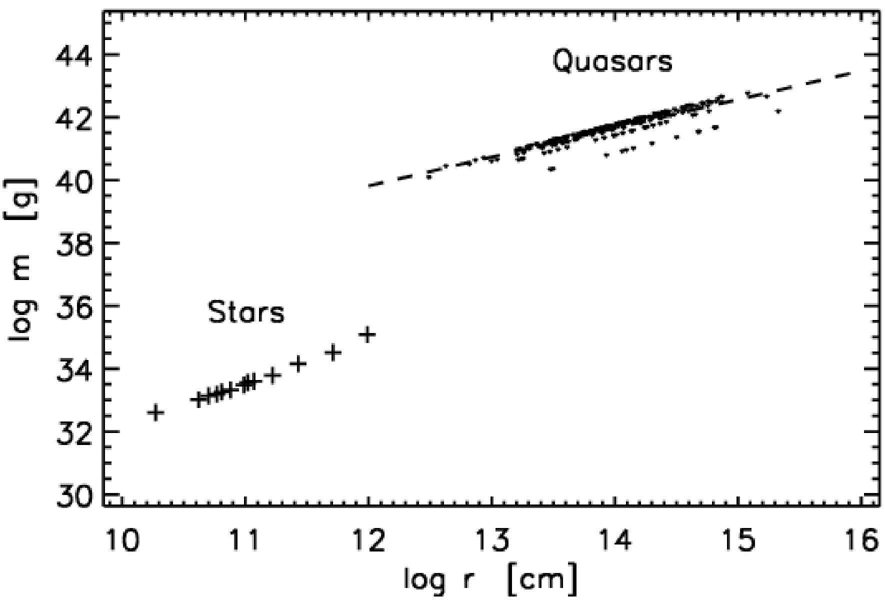

Figure 6. Diagram "mass - radius" for the sample of 225 local quasars (dots). The same relationship is shown also for stars (crosses), as mean values for: O5, B0, B5,.......,M5.

From eq.(14), more massive quasars have excessive luminosity, which could lead to extensive outer layers. This could be one possible reason for a relation of the type “mass – density” (see also Paper I), and which is shown in Fig (8) with data from Table 2. The mean line for quasars (correlation coeff.: - 0.79) is:

$$\log \rho_q = 67.59 - 1.65 \cdot \log m_q \tag{15}$$

In this case, the scatter of quasars compared to Paper I is more pronounced and the coefficients in eq. (15) deviate somewhat from the respective coefficients in Paper I. Possible causes for errors have been already mentioned above.

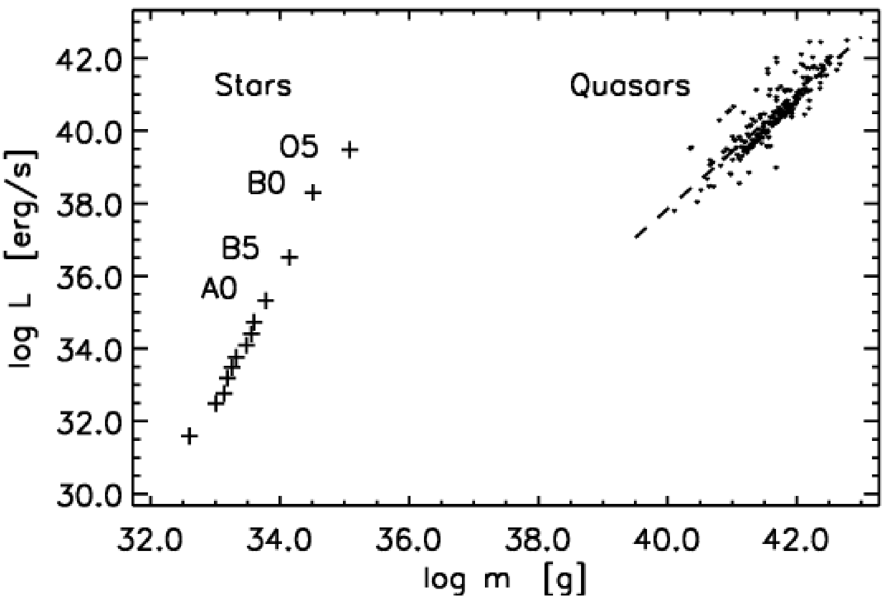

Figure 7. Diagram "mass - luminosity" for the sample of 225 local quasars (dots). The same relationship is shown also for stars (crosses), as mean values for: O5, B0, B5,.......,M5.

Eq.(15) implies that quasars of larger masses have smaller densities. Besides the possibility of extended outer layers, there could be another reason for this relation. We have already discussed the possibility of evolution of quasars due to disintegration of dense matter, which is inferred by Fig (1). A relation of the type as eq.(15) could also exist if the speed of evolution (disintegration) depends on the mass of the quasar: more massive quasars evolve more rapidly. Clearly, this question needs further study.

The picture presented in this study is self-consistent. However, there is a contradiction with some observational evidence. Host galaxies studies in [57, 58] revealed that host galaxies redshifts are identical with the redshifts of respective “hosted” quasars. On the other hand, a QSO is reported at only 2.4 arcsec from a dwarf galaxy [52]. Hotly debated is also a QSO (z=2.114) very close to the nucleus (and therefore, probably being hosted) of NGC7319 (z=0.022) [59]. Clearly, further studies would be needed.

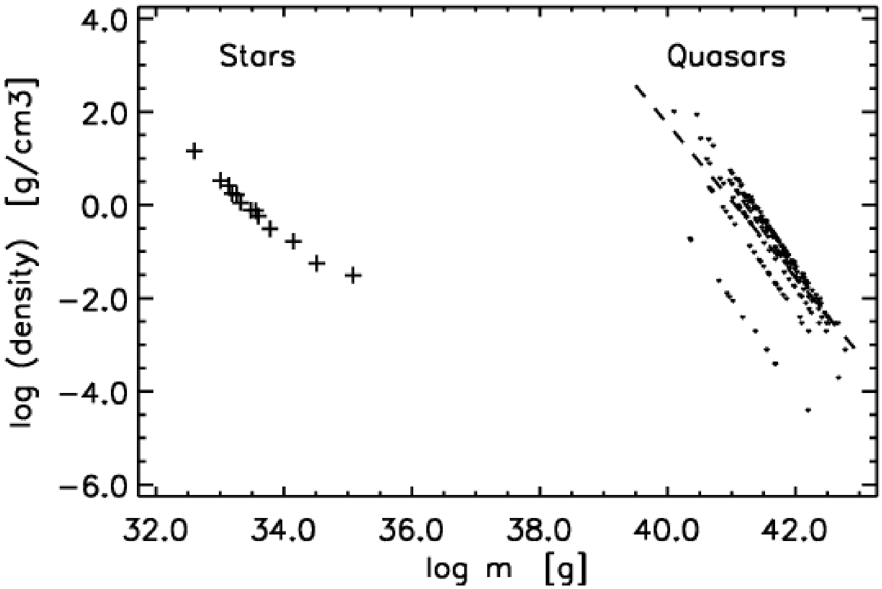

Figure 8. Diagram "mass - density" for the sample of 225 local quasars(dots). The same relationship is shown also for stars (crosses), as mean values for: O5, B0, B5,.....,M5. Note that the massive objects are now at the bottom of respective sequence.

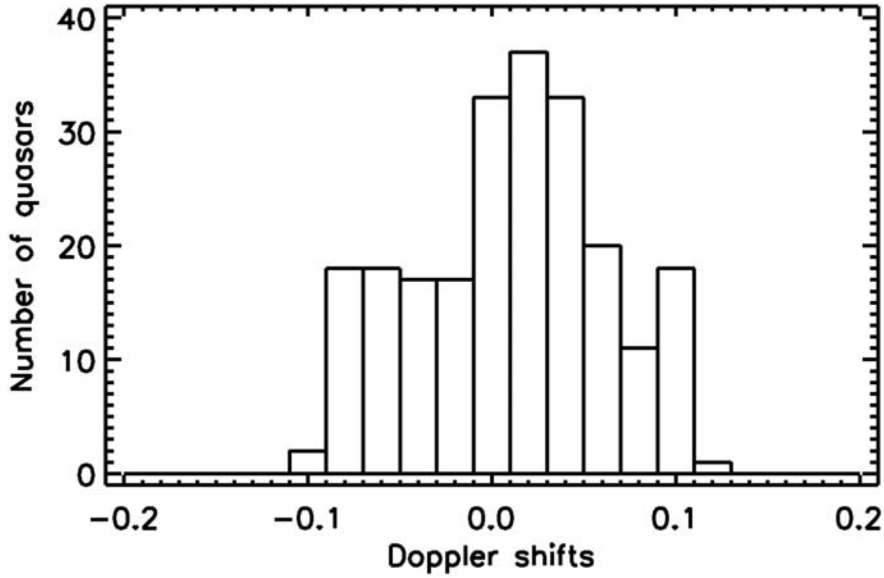

Figure 9. Distribution of the Doppler shifts of 225 possible local quasars (data from Table 2).

In Fig (9), the distribution of the Doppler-shifts of sample quasars is presented (data from Table 2). The real distribution is yet unknown but some general conditions could be considered:

- Doppler shifts reflect only the projections of ejection velocity along the line of sight;
- Lower ejection velocities are more likely than higher velocities. A peak in the distribution is therefore to be expected around the zero velocity, if the sample of quasars is large enough;
- Distribution should have symmetry with respect to the zero velocity, if all directions of ejection have the same probability. In some active galaxies, ejection of quasars has been reported along the rotational axis, i.e. along a preferred direction [28,29,37,52]. With a large sample of galaxies (and quasars), however, these effects should cancel out and the distribution should be symmetric;
- Ejection velocities should be limited.

From Fig (9), it is apparent that the peak of the distribution is shifted in direction of positive velocities. We believe, this is an effect of incompleteness of the sample. Also seen is the limiting Doppler shift, which is about 0.1 (maximal projected ejection velocity about 30 000 km.s^{-1}).

4. Conclusions

A sample of 225 possible local quasars from 18 active galaxies seems now to be established and all conclusions here refer only to these sample quasars. Generally, we could say that all relations for quasars found in Paper I could now be confirmed on a basis of larger sample. Local quasars are most probably ejected from respective parent galaxy. The maximal projected velocity of ejection found is about 30 000 km.s^{-1} .The physics of this ejection is yet unknown. The redshifts of quasars are probably a "mixture" of three components: gravitational reddening, cosmological component and Doppler component. The gravitational reddening seems to be the largest component and the cosmological redshift is that of the parent galaxy. Larger gravitational redshifts seem to correspond to fainter quasars. The gravitational redshifts are probably quantized, according to the Karlsson-sequence. Quasars behave like a single body. Their physical characteristics are listed in Table 2. A theory of such configurations does not yet exist. To understand quasars, we may need deeper knowledge of the atomic structure. Quasars from different galaxies are separated in radii and luminosities but the reason for that separation is not clear. In our sample, quasars of M82 are the least luminous and quasars of NGC4410 and NGC5548 are most luminous. Quasars seem to evolve with decreasing density and redshift (it is actually the gravitational component that depends on density). At large redshifts, the drop of redshift as density decreases is very fast. This could explain the well known problem of decline of number of quasars for $z > 3$. Density could possibly be decreasing because of disintegration of matter of yet unknown origin and properties. According to the Arp's scenario, quasars evolve into galaxies. Fig (1) and eq. (8), as well as Figs (2 and 3) fit quite well into this scenario and the conclusion would be that the evolution of quasars into galaxies proceeds with decreasing density and redshift but with increasing radius and luminosity.

In Fig (2) and Fig (3), the increase of luminosity by decreasing redshift is clearly seen. Quasars with the largest gravitational redshifts are also most young.

From the Arp's scenario, a fundamental question arises. If it is true that quasars evolve into galaxies, then some (compact) galaxies could still be in transition, meaning that they could also exhibit gravitational redshift component. It appears then that care should be taken to reduce possible gravitational redshifts when a Hubble diagram is constructed. This may turn to be a serious problem and the outcome is now unpredictable. However, the existence of local quasars does not exclude the possibility that other quasars are distant, at cosmological distances. The reduction of gravitational components in their redshifts would then be crucial.

This study confirms the previously found relations in Paper I: absolute mag – radius, absolute mag – mass, mass – radius, and mass – luminosity. The physics behind these relations is not yet clear. The remarkable feature is that all these relations exist also for stars, which has been known for many years. The tantalizing question arises, could there be a link between these seemingly entirely different kinds of objects? If yes, what is it? If no, how do we explain all these similar relations? Now, there is one more relation to come: the mass – density relation exists for quasars and also for stars. For quasars, it could be pointing to an evolution depending on the mass of the quasar: more massive quasars evolve (disintegrate) more rapidly. These parallels between quasars and stars are too many to be a coincidence. However, the consequences of these parallels could be far reaching.

An important, yet unsolved problem is the quantization of gravitational redshifts, according to the Karlsson-sequence. Some new studies with modern surveys did not confirm the Karlson-sequence. However, this negative result does not necessarily mean that this sequence does not exist. It may be that the sequence would be undetectable, because of more substantial contribution to the observed redshifts of the other two terms in the eq. (1): the cosmological term and the Doppler term. The contribution of the cosmological redshift will increase with distance, making any possible pattern in the gravitational redshifts undetectable. From Table 2, it is apparent that quantization of gravitational redshifts leads to a quantization of the ratio r_{gr}/r_q , and also to the quantization of reduced densities. This is well seen also in Fig (1). Arp [28] suggested that the evolution of redshifts proceeds in steps, each step corresponding to the next lower value of the Karlsson-sequence. If these results are confirmed, it could mean that we enter for the first time a quantized macro-world. A beguiling mirage or a reality? It remains to be seen.

In their last joint paper in the Astrophysical Journal [23], Burbidge and Napier reviewed the evidence for clustering of quasars near low redshift galaxies. In the present study, we believe, we could add some additional evidence about 225 possible local quasars. Disintegration processes of dense matter in the Universe may play far greater role than previously believed.

Acknowledgements For this work, we used the SIMBAD and Vizier databases, operated by CDS, Strasbourg, France.

References

[1] Antonucci R., 1993, *Unified models for active galactic nuclei and quasars*, AR Astron Astrophys ,31, 473-521.

[2] Djorgowski S.G., Volonteri M., Springel V., Bromm V., Meylan G., 2008,*The origins and the early evolution of quasars and supermassive black holes*, Proceed of XI Marcel Grossmann meeting on General Relativity

[3] Kembhavi A.K, Narlikar J.V., 1999 *Quasars and Active Galactic Nuclei: an introduction*, Cambridge University Press, Cambridge

[4] Lopez-Corredoira M., 2009, *Pending problems in QSOs*, arXiv 0910.4297 2009

[5] Lopez-Corredoira M., 2003, *Observational Cosmology: caveats and open questions in the standard model*, arXiv astro-ph/0310214 2003

[6] Wilson O.C., 1939, *Possible Applications of Supernovae to the Study of the Nebular Red Shifts*, Astrophys J ,90, 634-636

[7] Hawkins M.R.S., 2001, *Time Dilation and Quasar Variability*, Astrophys J., 553, L97-L100

[8] Karlsson K.G., 1971, *Possible Discretization of Quasar Redshifts*, Astron Astrophys 1971, 13, 333-335

[9] Karlsson K.G., 1977, On the existence of significant peaks in the quasar redshift distribution. Astron Astrophys ,58, 237-240

[10] Arp H., Bi H., Chu Y., Zhu X., 1990, *Periodicity of quasar redshifts*, Astron Astrophys, 239, 33-49

[11] Burbidge G., Napier W.M., 2001, *The Distribution of Redshifts in New Samples of Quasi-Stellar Objects*, Astron J., 121, 21-30

[12] Arp H.C., 1987, *Quasars, Redshifts , and Controversies. Interstellar Medium*, Berkley, USA

[13] Arp H.C., 2003, *Catalogue of discordant redshift associations*, APEIRON, Montreal, Canada

[14] Burbidge G., 1996, *The reality of anomalous redshifts in the spectra of some QSOs and its implications*, Astron Astrophys , 309, 9-22

[15] Burbidge G.R., 2001, *Noncosmological Redshifts*., Publ Astron Soc Pacific , 113, 899-902

[16] Hoyle F., Burbidge G., 1996, Anomalous redshifts in the spectra of extragalactic objects. Astron Astrophys , 309, 335-344

[17] Burbidge G., Hewitt A., Narlikar J.V., Gupta P. D., 1990, *Associations between quasi-stellar objects and galaxies*, Astrophys J. Suppl Ser ,74, 675-730

[18] Williams L.L.R, Irwin M., 1998, *Angular correlations between LBQS and APM: weak lensing by the large-scale structure*. Mon Not RAS , 298, 378-388

[19] Bell M.B., 2002, *Further Evidence for Large Intrinsic Redshifts*., Astrophys J.,566, 705-711.

[20] Jain B., Scranton R., Sheth R.K., 2003, *Quasar-galaxy and galaxy-galaxy cross-correlations: model predictions with realistic galaxies*. Mon Not RAS, 345, 62-70

[21] Nollenberg J.G., Williams L.L.R., 2005, *Galaxy-Quasar Correlations between APM Galaxies and Hambourg-ESO QSOs*, Astrophys J., 634, 793-805

[22] Lopez-Corredoira M., Gutierrez C.M., 2006, *Research on candidates for non-cosmological redshifts*, AIP Conf Proceed of First Crisis in Cosmology Conf, NY, USA, 822, 75-92

[23] Burbidge G., Napier W.M., 2009, *Associations of High-Redshift Quasi-Stellar Objects with Active, Low-Redshift Spiral Galaxies*, Astrophys J., 706, 657-664

[24] Lopez-Corredoira M., Gutierrez C.M., 2004, *The field surrounding NGC7603: Cosmological or non-cosmoloical redshifts?* Astron Astrophys, 421, 407-422

[25] Burbidge E.M., 1995, *Spectra of two quasars possibly ejected from NGC4258*, Astron Astrophys , 298, L1-L4

[26] Burbidge E.M., 1997, *Spectra of two X-Ray emitting Quasi-Stellar Objects apparenly ejected from the Seyfert Galaxy NGC2639*, Astrophys J. ,484, L99-L101

[27] Burbidge E.M., Burbidge G., 1997, *Ejection of Matter and Energy from NGC4258*, Astrophys J., 477,L13-L15

[28] Arp H., 1997, *Quasar Creation and Evolution into Galaxies*. J Astrophys Astron, 18, 393-406

[29] Arp H., 1997, *Pairs of X-ray sources across Seyferts: the NGC4235 field*, Astron Astrophys, 328, L17-L20

[30] Greenstein J.L., Schmidt M., 1964, *The Quasi-Stellar Radio Sources 3C48 and 3C273*. Astrophys J., 140, 1-37

[31] Hoyle F., Fowler W.A., 1967, *Gravitational Red-shifts in Quasi-Stellar Objects*, Nature ,213, 373-374

[32] Das P.K., 1976, *Physical properties of collapsed objects with large central gravitational redshifts*, Mon Not RAS, 177, 391-408

[33] Narlikar J.V., 1977, *Two Astrophysical Applications of Conformal Gravity*. Ann Phys, 107, 325-336

[34] Narlikar J.V., Arp H.C., 1993, *Flat Spacetime Cosmology – a Unified Framework for Extragalactic Redshifts*. Astrophys J. , 405, 51-56

[35] Panov K.P., 2011, *Study of Possible Local Quasars I. The First Sample*. OAJ ,4, 14-26.

[36] Arp H., 1998, *Evolution of Quasars into Galaxies and its implications for the birth and evolution of matter* ,APEIRON, 5, 135-142.

[37] Arp H., 1999, *Association of X-ray Quasars with Active Galaxies*, IAU Symp 183, 183, 290-295

[38] Veron-Cetty M.P., Veron P., 2010, *A catalogue of quasars and active nuclei: 13th edition*, Astron Astrophys ,518A, A10

[39] Gosset E., Moreau O., Surdej J., et al., 1997, *Surveys of ultraviolet-excess quasar candidates in large fields*, Astron Astrophys Suppl Ser ,123, 529-568

[40] Arp H, 2006, *Quasars associated with NGC613, NGC936 and NGC941*, Astrophys Sp Sci, 301, 117-126

[41] Arp H, Fulton C, Roscoe D.,2005, *Periodicities of Quasar Redshifts in Large Area Surveys*, arXiv astro-ph/0501090 2005.

[42] Burbidge E.M., 1999, *A group of quasi-stellar objects closely associated with NGC1068*, Astrophys J, 511, L9-L11.

[43] Arp H., Sulentic JW., 1979, *Three quasars near the spiral arms of NGC1073*, Astrophys J., 229, 496-502

[44] Kaaret P., 2005, *Optical Sources near the Bright X-Ray Source in NGC1073*, Astrophys J., 629, 233-238

[45] Arp H., 1998, *X-ray Observations of NGC1097 and Nearby Quasars* Astrophys Sp Sci , 262, 337-361

[46] Burbidge E.M., Burbidge G., Arp H.C., and Zibetti S., 2003, *QSOs associated with M82* Astrophys J.,591, 690-694

[47] Burbidge E.M., Burbidge G., Arp H.C., Napier W.M., 2005, *An anomalous concentration of QSOs around NGC3079*, arXiv astro-ph/10815 2005

[48] Arp H., Burbidge E.M., Chu Y et al., 2002, *NGC3628: Ejection activity associated with quasars*, Astron Astrophys 2002; 391: 833-840

[49] Arp H., Burbidge EM., Carosati D., 2006, *Quasars and Galaxy Clusters Paired Across NGC4410*, arXiv astro-ph/ 0605453 2006

[50] Zhu X., Chu Y., Wei J. et al., 2000, *A quasar possibly ejected from NGC4579*, Chinese Sci Bull , 45, 886-888

[51] Burbidge E.M., Burbidge G., 2002, *QSOs in the Field of the Seyfert1 Galaxy NGC5548*, Publ Astron Soc Pacific, 114, 253-256

[52] Arp H., 1999, *A QSO 2.4 arcsec from a dwarf galaxy – the rest of the story*, Astron Astrophys ,341, L5-L8

[53] Arp H., Russell D., 2001, *A Possible Relationship between Quasars and Clusters of Galaxies*, Astrophys J., 549, 802-819.

[54] Arp H.C., Burbidge E.M., Chu Y., Zhu X., 2001, *X-Ray-emitting QSOs Ejected from Arp 220*, Astrophys J., 553, L11-L13

[55] Burbidge G., 1996, *Two universes,* Astrophys Sp Sci , 244, 169-176

[56] Ambartsumian V.A., 1954, *On the Origin of Stars. Les Processus Nucleaires dans les Astres*, Commun 5-eme Coll Internat Astrophys Liege, 1, 293-300

[57] Canalizo G., Stockton A., 2000, *3C48: Stellar Populations and the Kinematics of Stars and Gas in the Host Galaxy*., Astrophys J., 528, 201-218

[58] Courbin F., Letawe G., Magain P. et al., 2002, *On-axis spatially resolved spectroscopy of low redshift quasar host galaxies: HE1503+0228, at z=0.135*, Astron Astrophys , 394, 863-872

[59] Galianni P., Burbidge E.M., Arp H., et al., 2004, *The discovery of a high redshift X-ray emitting QSO very close to the nucleus of NGC7319*, arXiv/astro-ph/0409215, 2004